# Bifurcation and Lorentz-Factor Scaling of Relativistic Magnetized Plasma Expansion

Edison Liang

*Rice University, Houston, Texas 77005-1892, USA*

Kazumi Nishimura

*Los Alamos National Laboratory, Los Alamos, New Mexico 87545, USA*
(Received 23 May 2003; revised manuscript received 30 January 2004; published 29 April 2004)

We report the long-term results of $2\frac{1}{2}$-dimensional particle-in-cell simulations of the relativistic expansion of strongly magnetized electron-positron plasmas. When the simulation is carried to $> 150$ light-crossing time of the initial plasma, the plasma pulse exhibits a number of remarkable properties. These include the repeated bifurcation of the pulse profile, development of a power-law momentum distribution with low-energy cutoff, and a simple scaling law for the peak Lorentz factor.

When a collisionless magnetic-dominated plasma [$\Omega_e/\omega_{pe} > 1$, $\Omega_e = eB/m_e c$ = electron gyrofrequency, $\omega_{pe} = (4\pi n e^2/m_e)^{1/2}$ = electron plasma frequency] surrounded by vacuum or low-density environment is suddenly deconfined, an intense electromagnetic (EM) pulse is released together with a self-induced drift current [1,2]. This current slows and reshapes the EM pulse so that it traps and accelerates the surface particles via the ponderomotive [3] and $\mathbf{J} \times \mathbf{B}$ forces. For an $e^+ e^-$ plasma, this mechanism, called the diamagnetic relativistic pulse accelerator (DRPA) [1], converts most of the initial magnetic energy into the ultrarelativistic directed energy of a fraction of the surface particles. The EM pulse pulls the trailing plasma with a leaky ponderomotive trap. This allows the EM pulse to continually shed slow tail particles and focus its acceleration on a decreasing number of fast particles, thereby becoming more relativistic with time [1].

However, previous simulations [1] stop at $t < 10L_0/c$ ($L_0$ = initial plasma thickness, $c$ = light speed; throughout this Letter all quantities are measured in the laboratory frame), unable to reveal the long-term behavior of the DRPA. Here we report new results from simulations that are carried to $> 150L_0/c$. Three unusual properties of DRPA are discovered: (a) the plasma pulse bifurcates repeatedly, leading to a complex, multipeak structure at late times; (b) the pulse particle momentum distribution evolves into a power law with low-energy cutoff; (c) the peak Lorentz factor of the momentum distribution increases as the square root of the number of gyroperiods. These results have important implications for gamma-ray bursts [4,5].

Figure 1 highlights the global evolution of a DRPA expanding into a vacuum in both slab and cylindrical geometries. In the following, we focus on the slab results since the cylindrical simulation cannot yet achieve the resolution of the slab case. Figure 2 gives the snapshots of the pulse structure, showing the bifurcation due to the formation of new ponderomotive traps in the dispersive

EM field. In these simulations, the bifurcation process begins at $t > 10L_0/c$, starting with the front of the pulse and repeats, leading to a complex multipeak structure at late times. Figure 2 insets show that each bifurcated density peak is associated with a current-reverse-current system, likely caused by gradient drifts. This bifurcation does not progress down to the plasma Debye length $c/\omega_{pe}$ (resolution limit of our particle-in-cell (PIC) simulations [6]). Preliminary Fourier analysis of bifurcated density profiles [e.g., Figs. 2(d) and 2(e)] of runs ranging from $L_0 = 120c/\Omega_e$ to $L_0 = 40\,000c/\Omega_e$ suggests that the dominant peaks have widths $\propto c\gamma_m(t_b)/(\text{few } \omega_{pe})$, where $\gamma_m(t_b)$ is a Lorentz factor of the EM pulse at the time of bifurcation $t_b$. Since $\gamma_m(t)$ increases with time (see below), peaks formed early are narrower than later-formed peaks (cf. Fig. 2). Eventually $c\gamma_m(t_b)/(\text{few } \omega_{pe})$ exceeds the overall pulse width $L(t)$ which increases more slowly and the bifurcation process stops globally. After this, the number of peaks stays constant or decreases slightly via mergers and dispersion. While we have not fully ascertained the mechanism for the bifurcation, the presence of the length scale $c\gamma_m(t_b)/(\text{few } \omega_{pe})$ hints that it may be related to nonlinear coupling of transverse EM modes and longitudinal modes. However, when radiation and radiation reaction (see below) are included, the bifurcation process may be modified or even terminated before it reaches the asymptotic state.

Simulations with additional nonaxial $B$ components and with the DRPA running into ambient plasmas produce more diverse pulse patterns. Figure 3 shows pulse structures from runs with nonzero $B_z$ and nonzero ambient density outside the expanding plasma. They demonstrate that (a) the DRPA is not inhibited by nonaxial components of $B$ that couple axial and radial motions, or by the interaction with cold ambient plasma; (b) the maximum Lorentz factor achieved in these cases are comparable to the benchmark of Fig. 2(a); (c) there is no 2D plasma instability at the DRPA interface with ambient cold plasma. Such instabilities may be
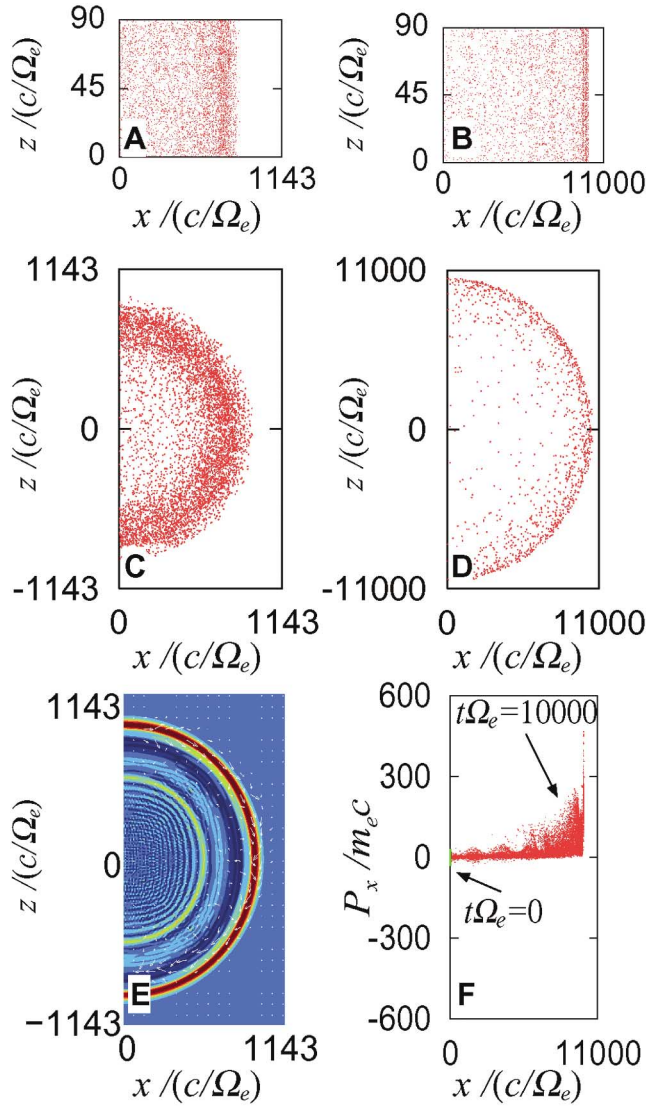
FIG. 1 (color).  $2\frac{1}{2}$-dimensional PIC simulations of slab and cylindrical magnetized relativistic $e^+e^-$ plasma expansion, comparing early and late times. Initial plasma temperature $kT = 5$ MeV, $\Omega_e/\omega_{pe} = 10$, initial slab width $L_0 = 120c/\Omega_e$, and uniform internal $\mathbf{B} = (0, B_0, 0)$. We show the $x \geq 0$ snapshots of particle distribution (a)–(d), axial magnetic field [color scale runs from $B_y = +0.2B_0$ (red) to $-0.1B_0$ (blue)] and current density (white arrows) for the cylindrical case (e), and phase plot for the slab case (f). $\Omega_e t = 800$ for all left panels and $\Omega_e t = 10^4$ for all right panels. The green dot in the phase plot denotes the initial phase volume. Results for $x < 0$ are identical.

suppressed by the strong transverse EM field of the pulse, and the DRPA mechanism survives because the acceleration rate exceeds the instability grow rates. Figures 3(b) and 3(c) also show that, when the ambient density is increased, low-energy "precursor" pulses of swept-up ambient plasma are produced ahead of the expanding high-energy plasma.
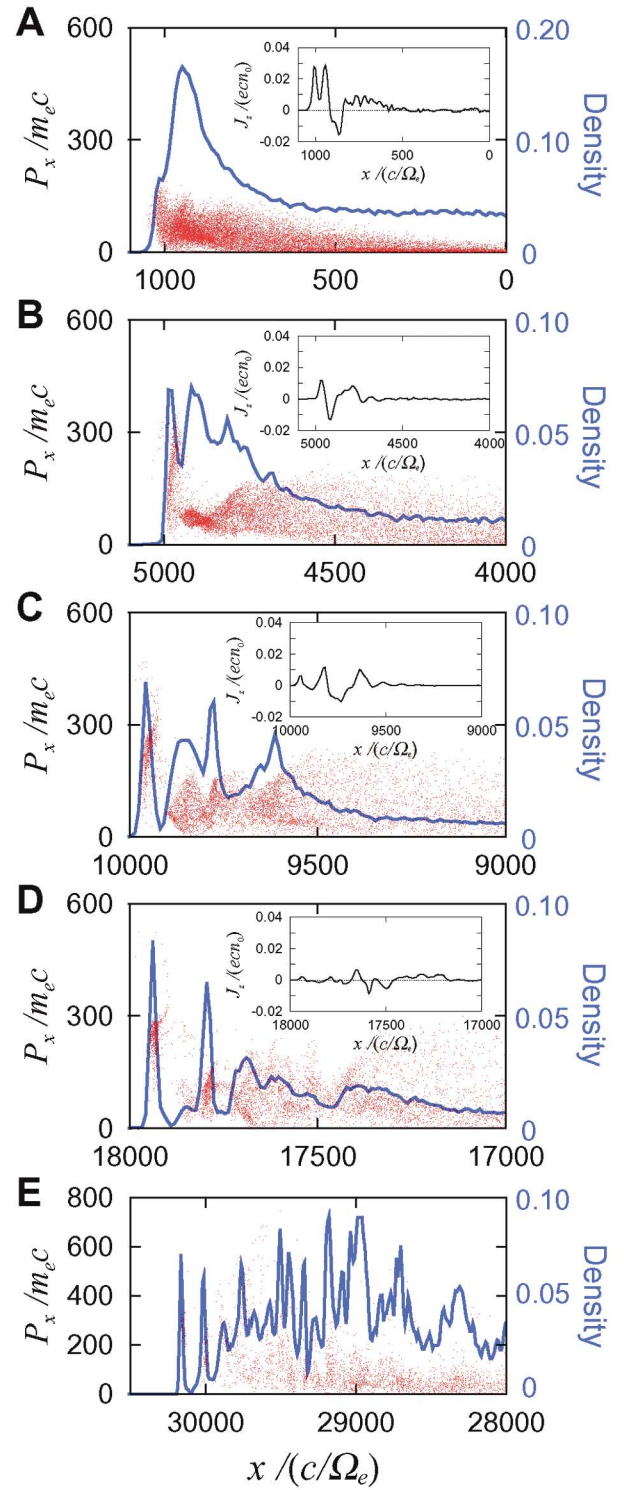


FIG. 2 (color).  Particle density profiles (blue curves, right scales) and phase plots (red dots, left scales) for the slab run of Fig. 1 at (a) $\Omega_e t = 1000$, (b) 5000, (c) 10 000, and (d) 18 000, with current densities in small insets. Panel (e) is the $\Omega_e t = 30\,000$ snapshot of another run with $L_0 = 600c/\Omega_e$, showing more peaks. These results may be relevant to GRB light curves and hard-to-soft spectral evolution [4,5].
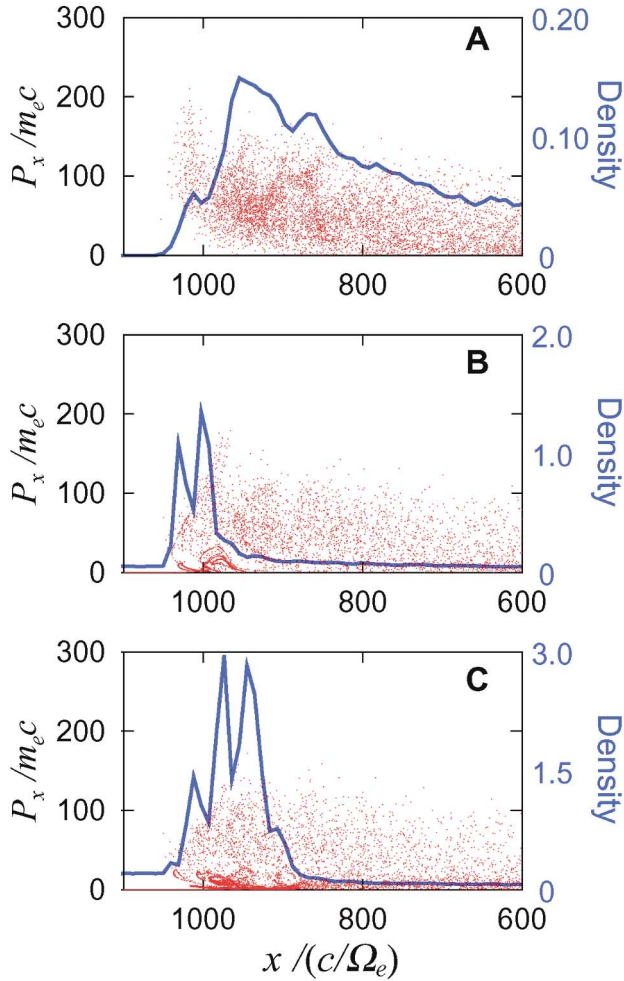
FIG. 3 (color). Particle density profiles (blue curves, right scales) and phase plots (red dots, left scales) at $\Omega_e t = 1000$ for runs with (a) $B_z$ increasing linearly from $B_z = 0$ at $x = 0$ to $B_z = B_0$ ($-B_0$) at $x = L_0/2$ ($-L_0/2$), (b) cold ambient $e^+ e^-$ density $= 5\%$ of slab density, and (c) cold ambient density $= 20\%$ of slab density. Other initial conditions are identical to Fig. 2(a).

As the DRPA of Fig. 2 advances, a peak develops in the momentum distribution of the front particles (Fig. 4). This peak Lorentz factor $\gamma_m = p_{x\max}/m_e c$ corresponds to the Lorentz factor of group velocity of the EM pulse, which is $< c$ due to plasma loading. Particles whose momenta lie below $p_{x\max}$ gradually lose acceleration and fall behind the EM pulse. This creates the deficit of low-energy particles in the front (Fig. 4 and Fig. 2 phase plots). At $\Omega_e t > 5000$, a power law develops above $p_{x\max}$. In this example, the power-law slope of $-3.5$ is close to the particle index of many astrophysical gamma-ray sources [5]. We also find that the power-law high-energy cutoff $\gamma_{\lim} \sim L(t)\Omega_e(t)/c$ [$\Omega_e(t) = $ gyrofrequency of the EM pulse peak at $t$]. When radiation (see below) is included, the power law may be truncated at an energy below $\gamma_{\lim}$ where acceleration equals radiation reaction.
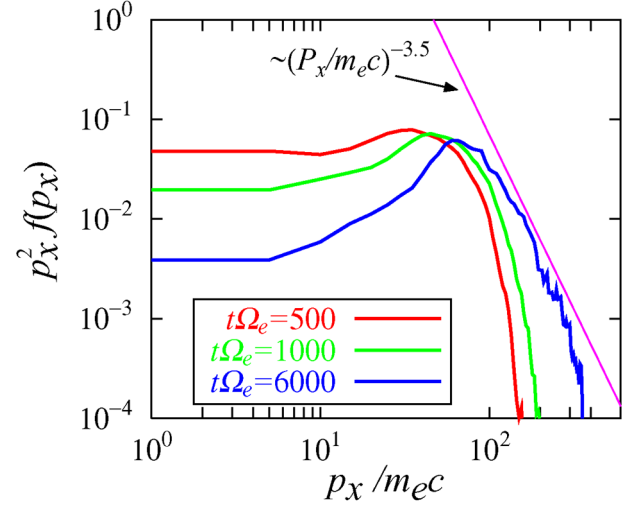
FIG. 4 (color online). Evolution of the $x$-momentum distribution for all surface particles in the slab pulse of Fig. 1, showing the development of the peak Lorentz factor $\gamma_m$ ($= p_{x\max}/m_e c$) and a power law with slope $\sim -3.5$.

The most important result from these long-duration simulations is the growth of the peak Lorentz factor $\gamma_m(t)$ with $t$ according to

$$\gamma_m(t) = [2f\Omega_e(t)t + C_0]^{1/2} \qquad t > L_0/c, \qquad (1)$$

where $C_0$ and $f$ are constants dependent on initial conditions (Fig. 5). We show that Eq. (1) can be derived from first principles.

Consider test particle motion in a 1D EM wave [7,8]. Define $(\beta_x, \beta_y, \beta_z) = d(x, y, z)/(cdt)$, and $eB(t, x)/m_e c = \Omega_e(t)h(\tau)$, where $\tau = t - x/\beta_w c$ is the retarded time with $\tau = 0$ at the peak of the pulse. $\beta_w$ ($< 1$) is the EM pulse profile speed/$c$. $h(\tau)$ is a normalized profile function so that $h(0) = 1$ and $h \to 0$ for $\tau \to +/-\infty$. The Lorentz force equation then becomes [7,8]

$$
\begin{aligned}
d(\gamma\beta_x)/dt &= -\beta_z\Omega_e(t)h(\tau); \\
d(\gamma\beta_z)/dt &= -(\beta_w - \beta_x)\Omega_e(t)h(\tau); \\
d(\gamma\beta_y)/dt &= 0,
\end{aligned}
\qquad (2)
$$

$$d\gamma/dt = -\beta_w\beta_z\Omega_e(t)h(\tau), \qquad (3)$$

where $(t, \tau)$ now replaces $(t, x)$ as independent variables and $\gamma = (1 - \beta^2)^{-1/2}$. We focus on particles that are comoving with the EM pulse so that $\beta_w = \beta_x$. Equations (2) can then be integrated to obtain

$$
\begin{aligned}
\beta_z &= -p_0/\gamma; \qquad \beta_y = p_0/\gamma; \\
\beta_x &= (\gamma^2 - 1 - 2p_0^2)^{1/2}/\gamma,
\end{aligned}
\qquad (4)
$$

$p_0$ is an integration constant corresponding to the initial isotropic momentum in the $z$ and $y$ directions. Note that the $z$ momentum is conserved because for comoving particles the **E** and **v×B** forces cancel exactly. Using
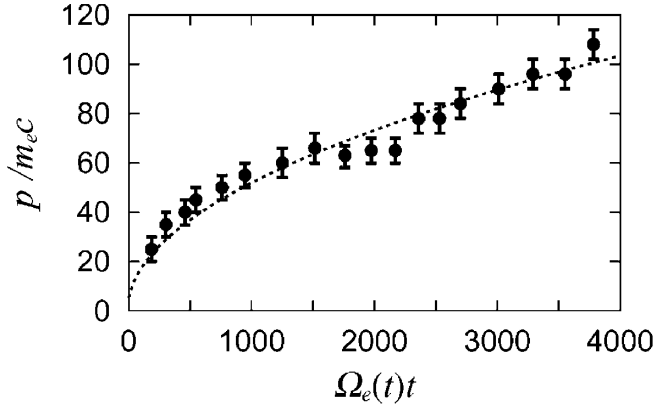
FIG. 5. The peak Lorentz factor $\gamma_m$ versus time for the slab pulse, compared with Eq. (1). The best-fit curve (dotted) gives $f = 1.33$ and $C_0 = 27.9$. [$\Omega_e(t)t = 3800$ is equivalent to $\Omega_e t = 18\,000$ due to $B$ decay.]

Eq. (4) in Eq. (3), we obtain

$$d\gamma^2/dt = 2p_0\Omega_e(t)h(\tau)\beta_x. \tag{5}$$

At large $\gamma$, $\beta_x = 1$ to lowest order. If we average Eq. (5) for all particles comoving with the pulse, this is equivalent to averaging $h$ in $\tau$, since the particles have random phases relative to the EM pulse. Hence, we have $d\langle\gamma^2\rangle/dt = 2p_0\Omega_e(t)\langle h\rangle$, which can be integrated to give $\langle\gamma^2\rangle(t) = 2f\Omega_e(t)t + \gamma_0^2$. This agrees with Eq. (1) if we identify $\gamma_m$ with $\langle\gamma^2\rangle^{1/2}$, and the constant $f$ depends on $\langle h\rangle$ and $p_0$. However, only a small fraction of the pulse particles are "comoving" with the EM pulse, and it depends on the field strength. In detailed parameter studies, we find that $f$ scales almost linearly with initial $\Omega_e/\omega_{pe}$.

The accelerated particles eventually lose energy and momentum via radiation, and Eqs. (2) and (3) must be modified to include radiation reaction, not included in the current PIC codes. We have compiled the acceleration histories of the pulse particles in our simulations and find that longitudinal acceleration ($\parallel p_x$) dominates transverse acceleration. Hence, DRPA radiates longitudinal "jitter" radiation [10] with a jitter length scale $\lambda \sim c\gamma/\Omega_e$. The total power output [8,9] is much below that of synchrotron [9] at the same $\gamma$. Using [8], we estimate the characteristic radiation frequency

$$\omega_{cr} \sim \gamma^2 c/\lambda \sim \gamma_m(t)\Omega_e(t). \tag{6}$$

While we defer astrophysical applications of these results to future publications [11], we point out here that Eqs. (1) and (6) lead to interesting numbers for gamma-ray bursts (GRBs) [12]. Typical long GRB durations are $\sim$30 s [4]. As an example, we assume that the GRB radiation time $t_r \sim 300$ s, since most GRBs have already bifurcated [4]. Equations (1) and (6) plus $h\omega_{cr}(t_r)/2\pi \sim$ 500 keV for the GRB spectral break [5] give $\gamma_m \sim$

few $10^7$ and $B \sim 10^6$ G. $B \sim 10^6$ G implies a magnetic energy $E_B(t_r) \sim 10^{50}$ ergs, assuming a $4\pi$ shell of thickness $L(t_r) \sim 10^{12}$ cm and radius $R \sim ct_r \sim 10^{13}$ cm. This gives a total initial energy [1] $E_{tot} \sim 10E_B(t_r) \sim 10^{51}$ ergs, consistent with GRB energetics [12,13]. If GRBs originate from a region $< 10^7$ cm, this magnetic energy implies an initial $B >$ few $10^{15}$ G, hinting at a magnetar connection [13]. If the recent polarization result [14] is confirmed, it would also favor a magnetic origin of GRBs [13].

[1] E. Liang *et al.*, Phys. Rev. Lett. **90**, 085001 (2003).
[2] A. Hasagawa and T. Sato, *Space Plasma Physics 1 Stationary Processes* (Springer-Verlag, Berlin, 1989).
[3] M. A. Miller, Radio Phys. **2**, 438 (1959); E. S. Weibel, J. Electron. Control **5**, 435 (1958).
[4] G. Fishman and C. A. Meegan, Annu. Rev. Astron. Astrophys. **33**, 415 (1995); G. Fishman, in *Compton Gamma-Ray Observatory*, edited by M. Friedlander *et al.*, AIP Conf. Proc. No. 280 (AIP, New York, 1993), p. 669.
[5] R. D. Preece *et al.*, Astrophys. J. Suppl. Ser. **126**, 19 (2000).
[6] C. K. Birdsall and A. B. Langdon, *Plasma Physics Via Computer Simulation* (IOP, Bristol, United Kingdom, 1991); K. Nishimura, S. P. Gary, and H. Li, J. Geophys. Res. **107**, SMP18-1 (2002).
[7] T. Boyd and J. Sanderson, *Plasma Dynamics* (Barnes & Noble, New York, 1969).
[8] L. Landau and E. M. Lifshitz, *Classical Theory of Fields* (Pergamon, London, 1965).
[9] M. V. Medvedev, Astrophys. J. **540**, 704 (2000).
[10] G. Rybicki and A. P. Lightman, *Radiative Processes in Astrophysics* (Wiley, New York, 1979).
[11] E. Liang, Astrophys. J. (to be published).
[12] See reviews by T. Piran, Phys. Rep. **333**, 529 (2000); P. Meszaros, Annu. Rev. Astron. Astrophys. **40**, 137 (2002).
[13] See, for example, M. V. Smolsky and V. V. Usov, Astrophys. J. **531**, 764 (2000); M. H. P. M. Van Putten and A. Levinson, Astrophys. J. **584**, 937 (2003); A. Levinson and M. H. P. M. Van Putten, Astrophys. J. **488**, 69 (1997); M. Lyutikov and R. Blandford, in Proceedings of the 1st Neils Bohr Summer Institute, edited by R. Ouyed *et al.* (astroph020671, 2003); M. Lyutikov and E. G. Blackman, Mon. Not. R. Astron. Soc. **321**, 177 (2002); E. G. Blackman, in Proceedings of the 1st Neils Bohr Summer Institute, edited by R. Ouyed *et al.* (astroph0211187, 2003).
[14] W. Coburn and S. E. Boggs, Nature (London) **423**, 415 (2003).